



Numerical demonstration of NAND and XNOR Boolean functions using quantum-dot semiconductor optical amplifiers-based turbo-switched Mach–Zehnder interferometers and delayed interferometer at 1 Tb/s

AMER KOTB^{1,2}^{*}, KYRIAKOS E ZOIROS³ and WEI LI^{1,*}

¹GPL, State Key Laboratory of Applied Optics, Changchun Institute of Optics, Fine Mechanics and Physics, Chinese Academy of Sciences, Changchun 130033, China

²Department of Physics, Faculty of Science, University of Fayoum, Fayoum 63514, Egypt

³Lightwave Communications Research Group, Department of Electrical and Computer Engineering, School of Engineering, Democritus University of Thrace, 67100 Xanthi, Greece

*Corresponding authors. E-mails: amer@ciomp.ac.cn; weili1@ciomp.ac.cn

MS received 22 September 2021; revised 8 December 2021; accepted 15 December 2021

Abstract. For the first time to our knowledge, the turbo-switched Mach–Zehnder interferometers (TS-MZIs) architecture, which includes quantum-dot semiconductor optical amplifiers (QDSOAs) and is followed by a series delayed interferometer (DI), is used in a combined scheme (QDSOAs-TS-MZIs-DI) to realise NOT-AND (NAND) and exclusive-NOR (XNOR) Boolean functions at a rate of 1 Tb/s return-to-zero data. The performance of the two considered gates is evaluated by calculating and comparing the quality factor and the cross-correlation coefficient for the QDSOAs-TS-MZIs-DI, the TS-MZIs with QDSOAs but without DI (QDSOAs-TS-MZIs) and the standard MZIs with QDSOAs (QDSOAs-MZIs). The comparison shows the superiority of the QDSOAs-TS-MZIs-DI over the other two alternatives (QDSOAs-TS-MZIs and QDSOAs-MZIs) and hence suggests that it should be preferred as a switching module when executing the NAND and XNOR Boolean functions at 1 Tb/s in the optical domain.

Keywords. Optical logic operations; quantum-dot semiconductor optical amplifier; turbo-switch; Mach–Zehnder interferometer; delayed interferometer.

PACS Nos 42.79.Sz; 85.35.Be; 85.30.-z

1. Introduction

With the growing requirement for faster data rates to cope with modern telecommunication networks' massive information capacity, quantum-dot semiconductor optical amplifiers (QDSOAs) are a promising alternative to conventional SOAs, which suffer from the slow dynamic response and the subsequent difficulty to operate at speeds exceeding 100 Gb/s. The most important characteristics that qualify QDSOA to replace the regular SOA are the more powerful saturation power, larger bandwidth, less noise figure, less thermal dependence [1–3] and, most importantly, faster gain response [4]. These unique properties make QDSOAs perfect candidates for implementing all-optical (AO) logic gates with acceptable performance at ultrafast data rates,

which their ordinary counterparts are not capable of [5–10]. Furthermore, an interferometric configuration that has widely been employed for exploiting the switching potential of nonlinear devices, like (QD-)SOAs, in the context of AO logic gates is the Mach–Zehnder interferometer (MZI), owing to its structural simplicity, controllable phase in each composing arm, small size, thermal stability, integrability and, overall, practicality [11]. Even better AO logic functionality can be achieved when the turbo-switched (TS) configuration is embedded in the conventional MZI, forming an enhanced new architecture referred to as the turbo-switched Mach–Zehnder interferometer (TS-MZI) [12–14]. The TS-MZI's ultrafast potential was recently paired with that of QD-SOAs by inserting the latter into the former to perform AO operations at 1 Tb/s [15,16]. On the other hand, a delayed interferometer (DI) can also extend

the speed of SOA-based AO Boolean logic functions [17,18]. It is thus rational to wonder whether combining the QDSOAs-TS-MZI with the DI would further facilitate the feasibility of realising AO gates in the Tb/s data regime. Thus, in this paper we employ the QDSOAs-TS-MZIs followed by a DI to numerically demonstrate the ultrafast performance of the AO NOT-AND (NAND) and exclusive-NOR (XNOR) logic operations at 1 Tb/s, for the first time to our knowledge, thus extending and complementing our previous studies in this regard [15,16]. For this purpose, our study compares three different schemes, i.e. the QDSOA-TS-MZIs-DI, the QDSOAs-TS-MZIs and the QDSOAs-MZIs, in terms of the quality factor (QF) and the cross-correlation (XC) coefficient, which are calculated for the considered operations at 1 Tb/s. The numerical outcomes show that using a DI after the QDSOAs-TS-MZIs is a favourable and subsequently preferable choice over both the QDSOAs-TS-MZIs and the QDSOAs-MZIs, as the NAND and XNOR Boolean functions can be investigated with much higher QF and XC at 1 Tb/s.

2. Modelling

2.1 QDSOAs-TS-MZIs-DI

Figure 1 shows the basic lay-out of the QDSOAs-TS-MZI followed by a DI [16]. In the QDSOAs-TS-MZI architecture, a pair of identical QDSOAs are cascaded and separated by optical bandpass filters (OFs) in each interferometric branch. The input signal to be switched at the output ('probe') is split into two copies, which enter the first concatenated QDSOAs and undergo cross-gain and cross-phase modulations subject to the concurrent presence of optical excitation ('pump'), which in the general case is applied to both QDSOAs. The following OFs pass only the dynamically modulated outcomes which reach the subsequent QDSOAs. The role of the additional QDSOAs is to offer a combined gain response much faster than the single devices. In this manner, the underlying nonlinear dynamical processes are accelerated, thereby allowing to strongly eliminate any pattern effects, which in turn is highly desirable for supporting operation at ultra-high speeds. The serially inserted DI, on the other hand, adds a phase difference to the direct and delayed copies of the incoming switched signal. As a result, a phase window is generated that is determined by the DI short delay ($\Delta\tau$) in one of its arms and phase bias ($\Delta\Phi$) in the other. This in turn enhances further the switching performance and speed of the formed AO gate.

The time-dependent gain equations used to model the response of each QDSOA, taking into account both interband and intraband nonlinear effects, are given by [7–10]

$$\frac{dh_d(t)}{dt} = \frac{h_w(t)}{\tau_{dw}} \left(1 - \frac{h_d(t)}{h_0} \right) - \frac{h_d(t)}{\tau_{dr}} - (\exp[h_d(t) + h_{CH}(t) + h_{SHB}(t)] - 1) \times \frac{P_{in,QDSOA_i}(t)}{E_{sat}}, \quad (1)$$

$$\frac{dh_w(t)}{dt} = \frac{h_{in}}{\tau_{wr}} \left(1 - \frac{h_w(t)}{h_0} \right) - \frac{h_w(t)}{\tau_{wr}} - \frac{h_w(t)}{\tau_{wd}} \left(1 - \frac{h_d(t)}{h_0} \right), \quad (2)$$

$$\frac{dh_{CH}(t)}{dt} = -\frac{h_{CH}(t)}{\tau_{CH}} - \frac{\varepsilon_{CH}}{\tau_{CH}} \times (\exp[h_d(t) + h_{CH}(t) + h_{SHB}(t)] - 1) \times P_{in,QDSOA_i}(t), \quad (3)$$

$$\frac{dh_{SHB}(t)}{dt} = -\frac{h_{SHB}(t)}{\tau_{SHB}} - \frac{\varepsilon_{SHB}}{\tau_{SHB}} \times (\exp[h_d(t) + h_{SHB}(t) + h_{CH}(t)] - 1) \times P_{in,QDSOA_i}(t) - \frac{dh_d(t)}{dt} - \frac{dh_{CH}(t)}{dt}, \quad (4)$$

$$h_{in} = \int_0^z \frac{a J \tau_{wr}}{ed} dz', \quad (5)$$

where h denotes the QDSOAs power gain integrated over their longitudinal dimension, $z \in [0, L]$, where L is the active region length, for carriers recombination between QDs states (h_d) and wetting layer (WL) (h_w), carrier heating (h_{CH}) and spectral hole burning (h_{SHB}). $h_0 = \ln[G_0]$, where the unsaturated power gain is G_0 and the saturation energy is E_{sat} . The excitation rate from QD ground state to WL is τ_{dw} and the recombination rate of QD is τ_{dr} . The transition rate from WL to QD ground state is τ_{wd} and the carrier recombination rate of WL is τ_{wr} . The temperature relaxation rate for CH is τ_{CH} and the carrier–carrier scattering rate for SHB is τ_{SHB} . The nonlinear gain suppression factors owing to CH and SHB, respectively, are ε_{CH} and ε_{SHB} . a is the differential gain, J is the injection current density, d is the WL thickness and e is the electron charge. The input power to each QDSOA engaged in the QDSOA-TS-MZI (denoted by index $i = 1, 2, 3, 4$) is $P_{in,QDSOA_i}(t)$. The time domain power profile of the excitation laser pulses of the QDSOAs is considered to be Gaussian, i.e. [15,16]

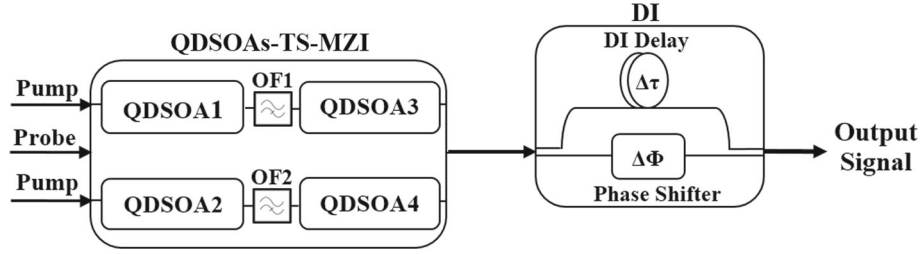


Figure 1. QDSOAs-TS-MZI schematic diagram with DI. OF: optical filter.

$$P_{A, B, \text{Clk}}(t) = \sum_{n=1}^N a_{n(A, B, \text{Clk})} \frac{2\sqrt{\ln[2]} E_0}{\sqrt{\pi} \tau_{\text{FWHM}}} \times \exp \left[-\frac{4 \ln[2](t - nT)^2}{\tau_{\text{FWHM}}^2} \right], \quad (6)$$

where $\alpha_{n(A, B, \text{Clk})}$ denotes the n th pulse of either excitation, i.e. data, signals (A, B), which are pseudorandom binary sequences (PRBS) of length $N = 2^7 - 1$ bit, or clock signal (Clk), i.e. $\alpha_{n(A, B)} = '1'$ or $'0'$ for A, B and $\alpha_{n(\text{Clk})} = '1'$ for the Clk. T is the signal bit period, E_0 is the pulse energy and τ_{FWHM} is the full-wave at half-maximum pulse width.

The overall gain of each QDSOA is then calculated using [15,16]

$$G_{\text{QDSOA}_i}(t) = \exp [h_d(t) + h_{\text{CH}}(t) + h_{\text{SHB}}(t)], \quad i = 1, 2, 3, 4 \quad (7)$$

while each QSOA's phase shift is determined by [15,16]

$$\Phi_{\text{QDSOA}_i}(t) = -0.5(\alpha h_d(t) + \alpha_{\text{CH}} h_{\text{CH}}(t) + \alpha_{\text{SHB}} h_{\text{SHB}}(t)), \quad i = 1, 2, 3, 4, \quad (8)$$

where α known as α -factor is the traditional linewidth enhancement factor. The linewidth enhancement factors owing to CH and SHB, respectively, are α_{CH} and α_{SHB} .

The optical power of the signal coming out of OF₁ and OF₂ and inserted into QDSOA₃ and QDSOA₄, respectively, is analogous to the square modulus of the corresponding electric field, $E_{\text{OF}_{1,2}}(t)$, i.e. [15,16]

$$P_{\text{in, QDSOA}_{3,4}}(t) \equiv P_{\text{OF}_{1,2}}(t) = |E_{\text{OF}_{1,2}}(t)|^2 = |F^{-1} \{ F [E_{\text{out, QDSOA}_{1,2}}(t)] \text{OF}_{1,2}[f] \}|^2, \quad (9)$$

where the Fourier transform and its inverse are represented by the operations F and F^{-1} , respectively. $E_{\text{out, QDSOA}_{1,2}}(t)$ is the electric field of the signal as it emerges from QDSOA₁ or QDSOA₂, as determined by [15,16]

$$E_{\text{out, QDSOA}_{1,2}}(t) = \sqrt{0.5 P_{\text{in, MZI}}} \times \exp [0.5 \ln [G_{\text{QDSOA}_{1,2}}(t)] + j \Phi_{\text{QDSOA}_{1,2}}(t)], \quad (10)$$

where $P_{\text{in, MZI}}$ is the power of the signal at MZI input. As it will be shown later, this power can be pulsed, i.e. Clk, or constant, i.e. continuous wave (CW), depending on the particular implementation of each considered gate. $G_{\text{QDSOA}_{1,2}}(t)$ and $\Phi_{\text{QDSOA}_{1,2}}(t)$ are the total gains and phase shifts of QDSOA₁ and QDSOA₂, respectively. The OF employed in this simulation is a Gaussian-shaped optical band-pass filter with a frequency domain field transfer function described by [15,16]

$$\text{OF}_{1,2}(f) = \exp \left[-\ln[\sqrt{2}] \left(\frac{f - f_c}{B/2} \right)^{2M} \right], \quad (11)$$

where f is the signal frequency, f_c is the centre frequency of the filter, B is the bandwidth of the filter. M is the order of the filter, which determines the sharpness of its passband edges [19], where $M = 1$ corresponds to Gaussian and $M \geq 2$ to super-Gaussian shapes. Then, the output power of QDSOAs-TS-MZI is given by [15,16]

$$P_{\text{QDSOAs-TS-MZI}}(t) = \left[|E_{\text{out, QDSOA}_3}(t)|^2 + |E_{\text{out, QDSOA}_4}(t)|^2 \right] / 2 \quad (12)$$

with

$$E_{\text{out, QDSOA}_{3,4}}(t) = E_{\text{OF}_{1,2}}(t) \exp [0.5 \ln [G_{\text{QDSOA}_{3,4}}(t)] + j \Phi_{\text{QDSOA}_{3,4}}(t)], \quad (13)$$

where $G_{\text{QDSOA}_{3,4}}(t)$ and $\Phi_{\text{QDSOA}_{3,4}}(t)$ are the total gains and phase shifts of QDSOA₃ and QDSOA₄, respectively.

The DI receives the output power given by eq. (12) and divides it into two equal parts, which go through the upper and lower arms of the DI. The output power given by eq. (12) is inserted in the DI and is divided into two equal parts travelling through the upper and lower arms

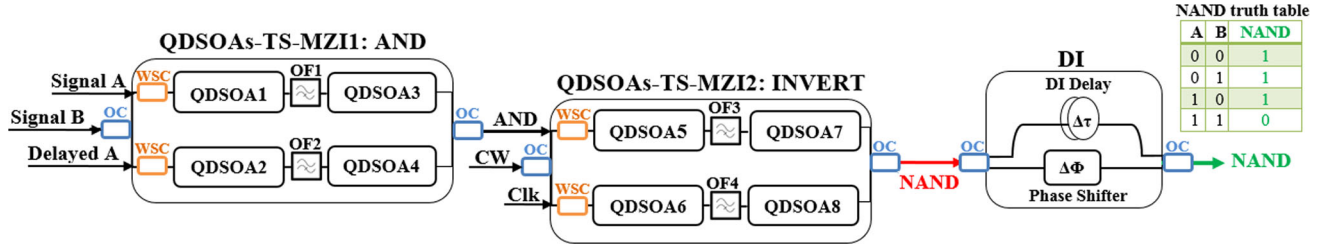


Figure 2. Schematic diagram and truth table of the NAND gate employing QDSOAs-TS-MZIs-DI. OC: 3 dB optical coupler, WSC: wavelength selective coupler, OF: optical filter, CW: continuous wave beam and Clk: clock signal (all ‘1’s).

of the DI. The output power of the DI is calculated as follows [16–18]:

$$P_{\text{out}}(t) = 0.25 \left(\frac{P_{\text{QDSOAs-TS-MZIs}}(t) + P_{\text{QDSOAs-TS-MZIs}}(t - \Delta\tau)}{-2\sqrt{P_{\text{QDSOAs-TS-MZIs}}(t) P_{\text{QDSOAs-TS-MZIs}}(t - \Delta\tau)} \cos [\Phi(t) - \Phi(t - \Delta\tau) + \Delta\Phi]} \right), \quad (14)$$

where $\Phi(t)$ is the function of the phase of the signal switched at QDSOA-TS-MZI output.

2.2 NAND gate

A succession of AND (QDSOAs-TS-MZI1) and INVERT (QDSOAs-TS-MZI2) gates combine to form the NAND gate between signals A and B [8]. The schematic diagram and truth table for this gate, which uses QDSOAs-TS-MZIs followed by a series DI, are shown in figure 2.

For the AND gate, the optical inputs to QDSOA-TS-MZI1 are such that signal A and its delayed replica are inserted in MZI1 upper and lower arms, respectively, acting as excitation signals, while signal B enters from the MZI1 middle port to change the dynamic properties of QDSOA_{1–4} caused by signal A and its delayed version. Therefore, the optical powers inserted into QDSOA₁ and QDSOA₂ are, respectively, expressed by [20]

$$P_{\text{in, QDSOA}_1}(t) = P_A(t) + 0.5 P_B(t), \quad (15)$$

$$P_{\text{in, QDSOA}_2}(t) = P_A(t - T_{\text{delay}}) + 0.5 P_B(t), \quad (16)$$

where T_{delay} is the time offset of signal A’s lagging copy.

For the INVERT gate, the optical inputs to QDSOAs-TS-MZI2 are such that the exit from the AND gate and a clock signal (Clk) are inserted in the upper and lower arms of the MZI2, acting as perturbation signals, while a continuous wave (CW) beam enters from the MZI2 middle port. The CW beam plays a two-fold role, i.e., functional and operational. In the first case, the product of switching is mapped on it and transferred at MZI2 output with the logical outcome of the NAND operation.

In the second case, it serves as a reference signal which,

by supplying extra power to the QDSOAs of MZI2, sets the saturation level of these active devices required for switching. This in turn gives permission to connect the AND gate directly to the INVERT gate by letting the former control the switching state of the latter without the need to use an extra amplification stage between them [12]. Therefore [20]

$$P_{\text{in, QDSOA}_5}(t) = P_{\text{QDSOAs-TS-MZI1}}(t) + 0.5 P_{\text{CW}}, \quad (17)$$

$$P_{\text{in, QDSOA}_6}(t) = P_{\text{Clk}}(t) + 0.5 P_{\text{CW}}, \quad (18)$$

where $P_{\text{QDSOAs-TS-MZI1}}$ is obtained from eq. (12) and P_{CW} is the CW beam power.

The input optical powers which are coming out of OF₃ and OF₄ and injected into QDSOA₇ and QDSOA₈ are, respectively, given by [15,16]

$$\begin{aligned} P_{\text{in, QDSOA}_{7,8}}(t) &\equiv P_{\text{OF}_{3,4}}(t) = |E_{\text{OF}_{3,4}}(t)|^2 \\ &= |F^{-1} \{ F [E_{\text{out, QDSOA}_{5,6}}(t)] \text{OF}_{3,4}[f] \}|^2 \end{aligned} \quad (19)$$

with

$$\begin{aligned} E_{\text{out, QDSOA}_{5,6}}(t) &= \sqrt{0.5 P_{\text{CW}}} \exp[0.5 \ln [G_{\text{QDSOA}_{5,6}}(t)] \\ &\quad + j \Phi_{\text{QDSOA}_{5,6}}(t)]. \end{aligned} \quad (20)$$

Then, the output power of QDSOAs-TS-MZI2 is given by

$$\begin{aligned} P_{\text{QDSOAs-TS-MZI2}}(t) &= \left[|E_{\text{out, QDSOA}_7}(t)|^2 + |E_{\text{out, QDSOA}_8}(t)|^2 \right] / 2. \end{aligned} \quad (21)$$

Finally, the NAND gate output power emerging from the DI is obtained from eq. (14) as

$$P_{\text{out}}(t) = 0.25 \left(\frac{P_{\text{QDSOAs-TS-MZI2}}(t) + P_{\text{QDSOAs-TS-MZI2}}(t - \Delta\tau)}{-2\sqrt{P_{\text{QDSOAs-TS-MZI2}}(t) P_{\text{QDSOAs-TS-MZI2}}(t - \Delta\tau)}} \times \cos[\Phi_{\text{NAND}}(t) - \Phi_{\text{NAND}}(t - \Delta\tau) + \Delta\Phi] \right), \quad (22)$$

where, similar to [13]

$$\Phi_{\text{NAND}}(t) = \arctan \left[\frac{\sqrt{G_{\text{QDSOA}_7}}(t) \sin[\Phi_{\text{QDSOA}_7}(t)] + \sqrt{G_{\text{QDSOA}_8}}(t) \cos[\Phi_{\text{QDSOA}_8}(t)]}{\sqrt{G_{\text{QDSOA}_7}}(t) \cos[\Phi_{\text{QDSOA}_7}(t)] - \sqrt{G_{\text{QDSOA}_8}}(t) \sin[\Phi_{\text{QDSOA}_8}(t)]} \right]. \quad (23)$$

2.3 XNOR gate

A succession of XOR (QDSOAs-TS-MZI1) and INVERT (QDSOAs-TS-MZI2) gates are used to create the XNOR gate between signals A and B [10]. The schematic diagram and truth table of the XNOR employing QDSOAs-TS-MZIs-DI are shown in figure 3.

The input optical powers going into QDSOA₁ and QDSOA₂ for XOR operation are stated as [20]

$$P_{\text{in, QDSOA}_1}(t) = P_A(t) + 0.5 P_{\text{CW}} \quad (24)$$

$$P_{\text{in, QDSOA}_2}(t) = P_B(t) + 0.5 P_{\text{CW}}. \quad (25)$$

The input powers to QDSOA₅ and QDSOA₆ for INVERT operation are expressed as follows [20]:

$$P_{\text{in, QDSOA}_5}(t) = P_{\text{QDSOAs-TS-MZI1}}(t) + 0.5 P_{\text{CW}} \quad (26)$$

$$P_{\text{in, QDSOA}_6}(t) = P_{\text{CLK}}(t) + 0.5 P_{\text{CW}}. \quad (27)$$

Then using eqs (19)–(23) but for inputs given by eqs (24)–(27), the XNOR gate output power emerging from the DI can be found by following the established computational procedure.

3. Results

The time-dependent equations used in the simulation of the NAND and XNOR logic gates were merged and numerically solved in Wolfram Mathematica using the Adams numerical method. The QF metric [5], which must be equal to at least six to provide acceptable performance [15,16], was used to evaluate the performance of the logic operations. Besides the QF, we also calculate the cross-correlation (XC) coefficient [21], which complements the pseudoeye diagrams (PEDs) by providing a measurement of the similarity degree between the logically outgoing pulses against the input ones. The higher the XC, the better the scheme’s capacity to reproduce the original input pulse (XC = 100% means

perfect match). The default values of the parameters that have been used herein are listed in table 1 [5–18].

The performance comparison of the NAND and XNOR logic operations at 1 Tb/s using QDSOA-TS-MZIs-DI, QDSOAs-TS-MZIs and QDSOAs-MZIs is depicted in figures 4–6 and 7–9, respectively. These results show the superiority of using a DI after QDSOAs-TS-MZI by obtaining higher QF than both QDSOAs-TS-MZIs and QDSOAs-MZIs. The numerically obtained XC values using QDSOAs-TS-MZIs-DI are 96% for the NAND and 93% for the XNOR. This means that the shape of the output pulses deviates only by 4 and 7%, respectively, from that at the QDSOAs input, which is also reflected on the quality of the corresponding PEDs. In contrast, the QF obtained with the QDSOAs-TS-MZIs is marginally acceptable, while the XC drops well below 90%, thus compromising the performance of both gates with this scheme. Moreover, the QDSOAs-MZIs show the worst switching behaviour among the three configurations employed to realise the considered AO gates, since the QF becomes unacceptable, while the XC is seriously deteriorated and along with it the corresponding PED. These results not only confirm the suitability of the TS architecture in assisting the NAND/XNOR operation of the QDSOAs-MZI modules but also support our proposal to use together with it the DI to significantly boost the performance of the considered gates.

The AO NAND and XNOR logic gates considered in this paper have recently been designed and theoretically demonstrated using other promising technologies, like plasmonic [22,23] and photonic crystal waveguides [24]. These nanoscale technologies feature ultracompact size, low latency, absence of heat dissipation, enhanced nonlinearity, noise-free operation and compatibility with conventional CMOS processing techniques. However, they suffer from inherent insertion losses, which can be compensated by using special waveguide structures and shapes at the expense of reduced cascability, and these waveguide structures depend on phase shifts, which makes them less

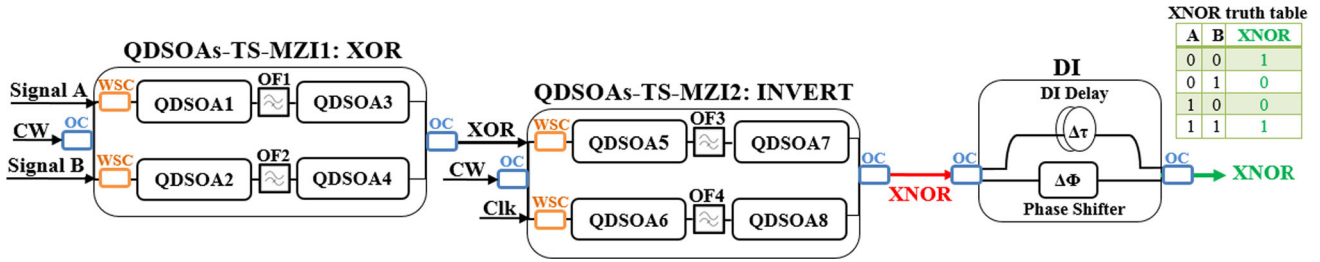


Figure 3. Schematic diagram and truth table of the XNOR gate employing QDSOAs-TS-MZIs-DI.

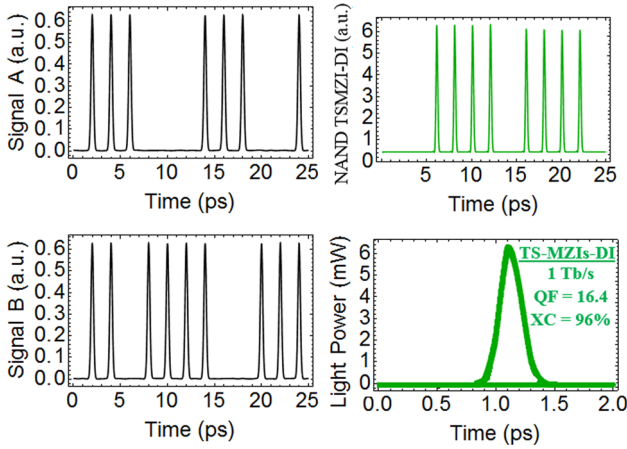


Figure 4. NAND results utilising QDSOAs-TS-MZIs-DI.

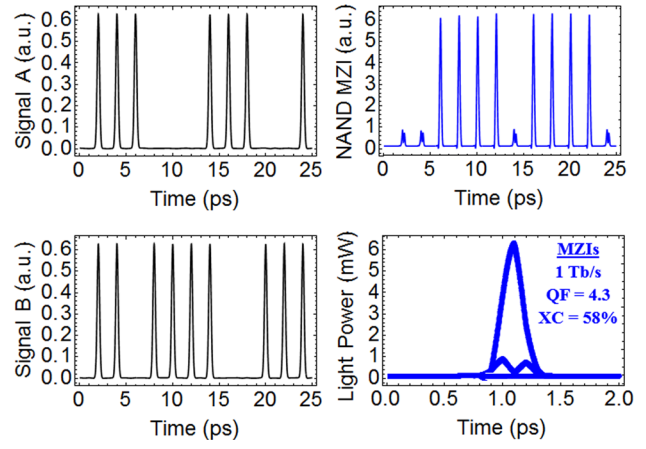


Figure 6. NAND results utilising QDSOAs-MZIs.

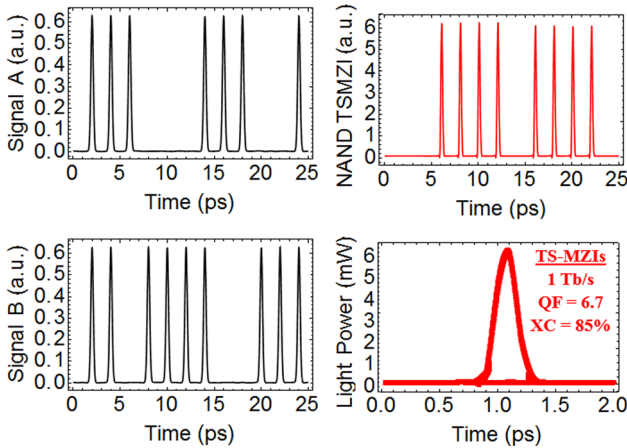


Figure 5. NAND results utilising QDSOAs-TS-MZIs.

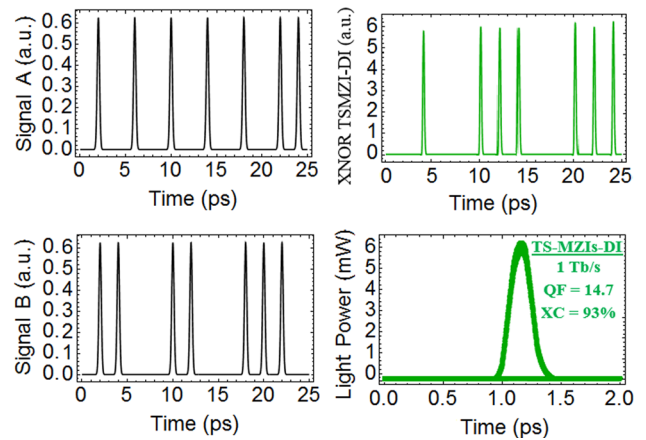


Figure 7. XNOR results utilising QDSOAs-TS-MZIs-DI.

transparent to different encoding formats, are less amenable to optical signal processing of multiple information channels and require further investigation before they can become a viable solution.

Furthermore, although these schemes claim to be capable of ultrafast operation based on their calculated or measured time-domain switching responses, whose inverse determines the maximum bit rate that they can handle, yet in the majority of cases this is not

supported by reported results and performance metrics under dynamic conditions, such as switching data pattern profiles with corresponding eye diagrams and QF but only by static characterisation, which is not sufficient in the context of the diverse and demanding applications that AO gates intend to serve. On the other hand, the proposed QDSOAs-TS-MZIs-DI does not face the aforementioned practical limitations or lack of solid evidence, as it effectively combines the well-established functions of the MZI and DI modules, in particular, the

Table 1. Default values of the parameters [5–18].

Symbol	Definition	Value	Unit
E_0	Pulse energy	20	fJ
τ_{FWHM}	Pulse width	0.3	ps
T	Bit period	1	ps
N	PRBS length	127	–
T_{delay}	Time delay of delayed signal A (AND operation)	0.15	ps
f_A	Frequency of signal A (AND operation)	193.5	THz
$f_{\text{delayed A}}$	Frequency of delayed signal A (AND operation)	193.5	THz
f_B	Frequency of signal B (AND operation)	192.9	THz
f_A	Frequency of signal A (XOR operation)	194.2	THz
f_B	Frequency of signal B (XOR operation)	193.5	THz
f_{CW}	Frequency of CW	192.8	THz
f_{Clk}	Frequency of Clk	192.9	THz
f	Filter centre frequency	194.7	THz
B	Filter optical bandwidth	1.8	THz
M	Filter order	2	–
I	Injection current	200	mA
P_{sat}	Saturation power	30	mW
τ_{wd}	Transition rate from WL to QDs state	5	ps
τ_{dw}	Excitation rate from QDs state to WL	10	ns
τ_{wr}	Carrier recombination rate in WL	2.2	ns
τ_{dr}	Carrier recombination rate in QDs state	0.4	ns
τ_{CH}	Temperature relaxation rate	0.3	ps
τ_{SHB}	Carrier–carrier scattering rate	0.1	ps
α	α -Factor	5	–
α_{CH}	CH linewidth enhancement factor	1	–
α_{SHB}	SHB linewidth enhancement factor	0	–
ε_{CH}	CH nonlinear gain suppression factor	0.02	W^{-1}
ε_{SHB}	SHB nonlinear gain suppression factor	0.02	W^{-1}
Γ	Optical confinement factor	0.15	–
a	Differential gain	8.6×10^{-15}	cm^{-2}
d	Thickness of WL	0.2	μm
L	Length of QDSOA active region	1	mm
G_0	Unsaturated power gain	30	dB
$\Delta\tau$	DI relative delay	0.1	ps
$\Delta\Phi$	DI phase bias	π	rad

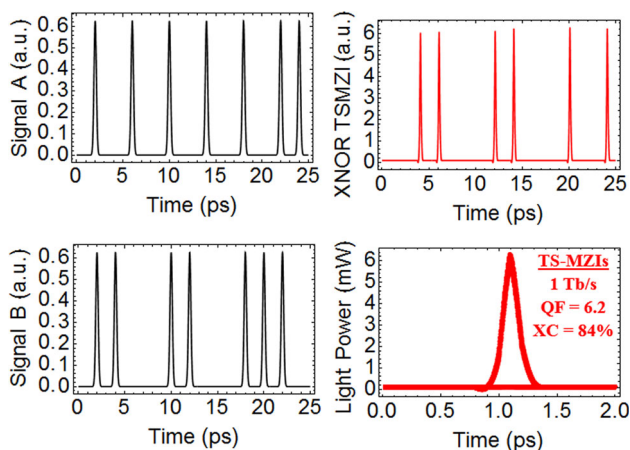


Figure 8. XNOR results utilising QDSOAs-TS-MZIs.

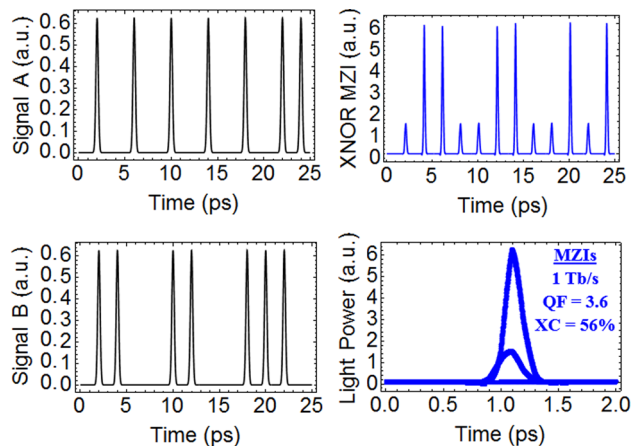


Figure 9. XNOR results utilising QDSOAs-MZIs.

inherent regeneration potential of the former and the adjustable switching window width of the latter, with the proven speed acceleration and photonic integration of the TS architecture [25] and the notably fast response and wideband high gain of QD-SOA devices whose technology is rapidly maturing [26,27]. By combining these assets into a unified platform, the specific scheme, provided that it is properly designed, can guarantee the execution of the target AO logic gates at repetition rates in the Tb/s regime with high performance.

4. Conclusion

In this paper, we conducted a numerical assessment of the ultrafast performance of all-optical NAND and XNOR logic gates at 1 Tb/s using QDSOAs-TS-MZIs followed by a series DI. Performance comparison of QDSOAs-TS-MZIs-DI, QDSOAs-TS-MZIs and QDSOAs-MZIs for the considered logic operations was realised by evaluating the QF and XC metrics. The obtained results indicated that the NAND and XNOR Boolean functions can be realised at 1 Tb/s with much higher QF and XC using QDSOAs-TS-MZIs-DI than QDSOAs-TS-MZIs and QDSOAs-MZIs.

Acknowledgements

This research was supported by the Chinese Academy of Sciences President's International Fellowship Initiative (Grant No. 2022VMB0013).

References

- [1] T W Berg and J Mørk, *IEEE Quantum Electron.* **40**, 1527 (2004)
- [2] T Akiyama, M Ekawa, M Sugawara, K Kawaguchi, H Sudo, A Kuramata, H Ebe and Y Arakawa, *IEEE Photon. Technol. Lett.* **17**, 1614 (2005)
- [3] N Yasuoka, K Kawaguchi, H Ebe, T Akiyama, M Ekawa, K Morito, M Sugawara and Y Arakawa, *IEEE Photon. Technol. Lett.* **20**, 1908 (2008)
- [4] A J Zilkie, J Meier, M Mojahedi, P J Poole, P Barrios, D Poitras, T J Rotter, C Yang, A Stintz, K J Malloy, P W E Smith and J S Aitchison, *IEEE Quantum Electron.* **43**, 982 (2007)
- [5] S Ma, Z Chen, H Sun and N K Dutta, *Opt. Express* **18**, 6417 (2010)
- [6] A Rostami, H Nejad, R Qartavol and H Saghai, *IEEE Quantum Electron.* **46**, 354 (2010)
- [7] E Dimitriadou and K E Zoiros, *Opt. Laser Technol.* **44**, 1971 (2012)
- [8] A Kotb and K E Zoiros, *J. Comput. Electron.* **13**, 555 (2014)
- [9] E Dimitriadou and K E Zoiros, *Opt. Laser Technol.* **45**, 79 (2013)
- [10] A Kotb, *Braz. J. Phys.* **45**, 288 (2015)
- [11] R P Schrieck, M H Kwakernaak, H Jäckel and H Melchior, *IEEE Quantum Electron.* **38**, 1053 (2002)
- [12] I Rendón-Salgado, E Ramírez-Cruz and R Gutiérrez-Castrejón, *Opt. Laser Technol.* **109**, 671 (2019)
- [13] I Rendón-Salgado and R Gutiérrez-Castrejón, *Opt. Commun.* **399**, 77 (2017)
- [14] R Gutiérrez-Castrejón, *Opt. Commun.* **282**, 4345 (2009)
- [15] A Kotb, K E Zoiros and C Guo, *J. Comput. Electron.* **18**, 628 (2019)
- [16] A Kotb and C Guo, *Optik* **218**, 164879 (2020)
- [17] A Kotb, K E Zoiros and C Guo, *Photon. Netw. Commun.* **38**, 177 (2019)
- [18] A Alquliah, A Kotb, S C Singh and C Guo, *Optik* **25**, 165901 (2021)
- [19] E Dimitriadou and K E Zoiros, *J. Lightwave Technol.* **31**, 3813 (2013)
- [20] A Kotb, *Opt. Quantum Electron.* **49**, 281 (2017)
- [21] Z V Rizou, K E Zoiros and A Hatziefremidis, *Appl. Sci.* **7**, 783 (2017)
- [22] S Swarnakar, S K Reddy, R Harijan and S Kumar, *Opt. Quantum Electron.* **53**, 493 (2021)
- [23] K Choudhary, S Mishra, S Singh and S Kumar, *Proc. SPIE* **11680**, 116801J (2021)
- [24] D G S Rao, S Swarnakar and S Kumar, *Opt. Eng.* **59**, 057101 (2020)
- [25] T Cassese, N Andriolli, C Porzi, X Yang and G Contestabile, *Proc. Asia Communications and Photonics Conference*, paper S4J.4 (2017)
- [26] J C Norman, D Jung, Y Wan and J E Bowers, *APL Photon.* **3**, 030901 (2018)
- [27] H G Yousefabad, S Matloub and A Rostami, *Sci. Rep.* **9**, 12919 (2019)